ACS Chemical Neuroscience

pubs.acs.org/chemneuro Research Article

An Isoquinolinium Dual Inhibitor of Cholinesterases and Amyloid β Aggregation Mitigates Neuropathological Changes in a Triple-Transgenic Mouse Model of Alzheimer's Disease

Yaojun Ju, Harapriya Chakravarty, and Kin Yip Tam*

Cite This: https://dx.doi.org/10.1021/acschemneuro.0c00464 Read Online

ACCESS | Metrics & More | Article Recommendations

ABSTRACT: Alzheimer's disease (AD) is a complex neurodegenerative disorder affecting millions of people worldwide. The underlying pathologic mechanisms of AD are unclear. Over the decades, the development of single target agent did not lead to any successful treatment for AD. A multitarget agent that could tackle more than one AD phenotype may be helpful as a treatment strategy. Cholinesterases (ChEs) including acetylcholinesterase (AChE) and butyrylcholinesterase (BuChE), are currently the drug targets with approved treatments. Moreover, amyloid beta (Aβ) deposition is a hallmark of AD that receives considerable attention. Herein, **9Q**, a previously reported dual target inhibitor dealing with cholinergic dysfunction and amyloid deposition for AD treatment, has undergone thorough investigations. *In vitro* studies revealed that **9Q** exhibited over 80% inhibition of ChE activity at 100 μM and more than 30% inhibition of Aβ aggregation at 1 mM concentration. Moreover **9Q** was able to penetrate the blood−brain barrier (BBB) and enhance the cerebral acetylcholine level in triple transgenic AD (3xTg-AD) mice. Following one month treatment with **9Q**, the amyloid burden and the cognitive deficits in 3xTg-AD mice were significantly ameliorated. It was observed that **9Q** treatment mitigated synapse dysfunction, decreased amyloidogenic APP processing, and reduced the tau pathology in 3xTg-AD mice. Taken together, our results suggested that dual inhibition of cholinesterases and Aβ aggregation could be a promising approach in AD treatment.

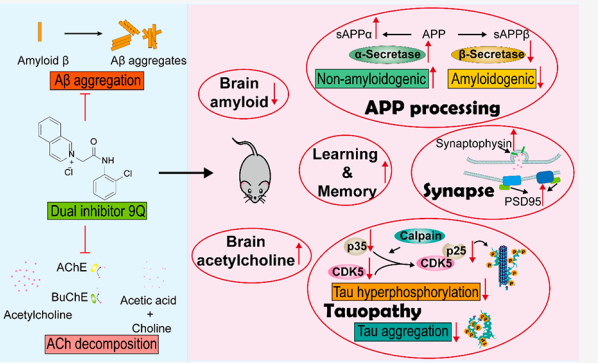

KEYWORDS: *cholinesterase, amyloid beta, dual inhibition, Alzheimer's disease*

1. INTRODUCTION

Alzheimer's disease (AD) accounts for most age-related dementia cases with number predicted to reach 131.5 million by 2050.[1] It has brought heavy financial burden to many countries around the globe. Though considerable efforts have been made to discover therapeutic interventions, AD remains inexorable and incurable. By now, only a few FDA approved drugs are available to offer limited cognitive improvement.[2] The underlying pathologic mechanisms of this disease are unclear.[3] Cholinergic dysfunction, amyloid plaques, neurofibrillary tangles, neuroinflammation, and mitochondrial dysfunction, as well as oxidative stress, are the major hallmarks of AD. For decades, the "one drug for one target" strategy has been undertaken in the development of treatment approachs, but this was unable to conquer this multifactorial disease. It has been suggested that pleiotropic agents which are capable of simultaneously interacting with several pathologies, could be effective in AD treatment.[4]

It has been reported that decreased choline acetyltransferase activity, decreased cholinergic transmission, and cholinergic neuron atrophy were correlated with dementia severity.[5] Cholinergic dysfunction was the first hypothesis for AD pathology. Donepezil, rivastigmine, galantamine, and memantine are currently the only four AD drugs available in clinics. The former three are acetylcholinesterase inhibitors (AChEI) while the latter is an *N*-methyl-D-aspartate receptor (NMDAR) antagonist, which could modulate the symptoms of AD to a certain extent.[2] It is noted that AChEIs (donepezil, rivastigmine, and galantamine) account for most of the FDA approved AD drugs. AChEIs decrease the acetylcholinesterase (AChE) activity in AD patients' brains, impede cerebral acetylcholine metabolism, and prolong acetylcholine action at the synapses.[6] Butyrylcholinesterase (BuChE) also plays an important role in the hydrolysis of acetylcholine in normal

Received: July 22, 2020
Accepted: September 21, 2020

brains.[7,8] In addition, BuChE was found to be associated with AD pathology, such as amyloid beta (Aβ) plaques, a major hallmark of AD.[9−11] Thus, inhibition of AChE and BuChE could be useful to enhance the symptomatic treatment of AD.

Among other hallmarks, Aβ is an important pathological target due to its predominant role in AD pathology.[12] In a pathological condition, amyloid precursor protein (APP) is catalyzed by β-secretase and γ-secretase to produce Aβ via the amyloidogenic pathway. In physiological conditions, α-secretase instead of β-secretase processes APP to form soluble APPα fragment via the nonamyloidogenic pathway.[13,14] The deposition of Aβ was thought to initiate a series of AD pathologies, including senile plaques, neurofibrillary tangles, neuron death, and dementia.[15] Accumulating evidence suggests that amyloid oligomers are the major cause of neurotoxicity.[16,17] Designing inhibitors targeting amyloid aggregation has been one of the desirable approaches to reduce Aβ accumulation and toxicity in AD brains.[18,19]

Recently, the application of multitarget-directed ligands (MTDLs) has been reported as a very powerful and promising approach to tackle AD.[20,21] AChEI-based MTDLs were reported to modulate the disease by not only enhancing the acetylcholine action but also inhibiting Aβ aggregation and scavenging oxygen radicals.[22−24] In the present study, we carried out extensive pharmacological evaluation of a previously reported dual inhibitor of ChEs and Aβ aggregation, **9Q** (see Figure 1),[25] using *in vitro* models and triple transgenic

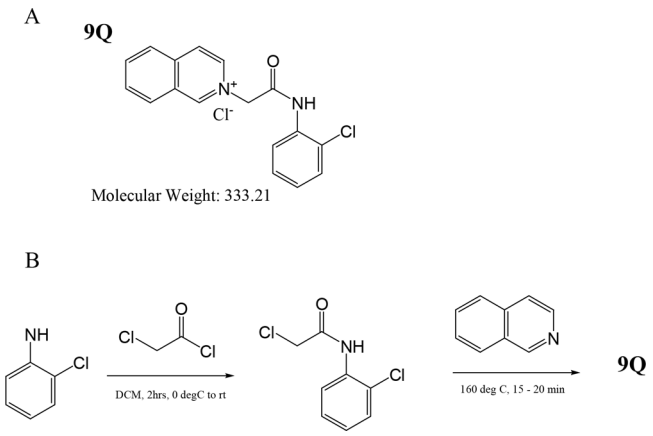

Figure 1. (A) Chemical structure of **9Q**. (B) Synthetic scheme of **9Q**.

AD (3xTg-AD) mouse model. Cerebral accumulation of **9Q** and the acetylcholine content in mouse brains were determined to evaluate, respectively, the blood−brain barrier (BBB) penetration ability of **9Q** and the enhancement of acetylcholine *in vivo*. The Morris water maze (MWM) was used to assess the cognitive impairments of the 3xTg-AD mice after 1 month treatment with **9Q**. The expression levels of different AD pathological proteins in **9Q** treated mouse brains were studied using immunoassays, including enzyme-linked immunosorbent assay (ELISA), Western blot assay, immunohistochemistry (IHC), and immunofluorescence (IF). The neuroprotective effects of **9Q** against tau hyperphosphorylation were demonstrated using the SH-SY5Y cell model.

2. RESULTS

2.1. Compound 9Q Suppressed *in Vitro* ChE Activity and Aβ Aggregation and Exhibited Low Cytotoxicity.

The *in vitro* ChE inhibitory effect of **9Q** was evaluated using Ellman's method. Donepezil, the FDA approved cholinesterase inhibitor for treating AD, was used as the positive control. The IC_{50} values of **9Q** on AChE and BuChE were determined as 1.68 μM and 16.34 μM, respectively (see Figure 2A). Compound **9Q** exhibited over 80% inhibition on both AChE and BuChE at a concentration of 100 μM. It is noted that **9Q** outperformed donepezil in BuChE inhibition.

In order to test the *in vitro* inhibitory effect of **9Q** on Aβ aggregation, the MALDI-TOF MS instrument was used to monitor residual monomeric Aβ42 in the aggregation solutions. Tramiprosate,[26] an Aβ aggregation inhibitor in phase III clinical evaluation, was used as positive control. As shown in Figure 2B, **9Q** significantly inhibited the aggregation of Aβ42 compared with the vehicle control ($F(2,15) = 15.25$, $p = 0.0002$). Compound **9Q** (1 mM) showed 36.3% inhibition of Aβ aggregation, outperforming tramiprosate at the same concentration.

To assess the toxicity of **9Q**, MTT assay was used to evaluate the cell viability of SH-SY5Y cells upon incubation with the compound for 24 h. Compound **9Q** showed minimal toxicity even at 200 μM compared with the vehicle control containing the same amount of DMSO (see Figure 2C).

2.2. Compound 9Q Penetrated the BBB and Enhanced the Cerebral Acetylcholine Level in 3xTg-AD Mice.

To explore the ability of **9Q** to cross the BBB, brain deposition of **9Q** was studied in 3xTg-AD mice. Following IP dosing of **9Q** (10 mg/kg), the plasma and brain samples were harvested after 120 min. The concentrations of **9Q** were found to be 3.04 ± 1.54 ng/mL (mean ± SD, $n = 10$) in plasma and 4.65 ± 4.35 ng/g (mean ± SD, $n = 10$) in brain. To study the *in vivo* ChE inhibitory effect of the compound, the cerebral acetylcholine level was determined after 120 min from IP dosing (10 mg/kg **9Q**). The cerebral acetylcholine levels in PBS control and **9Q** group were found to be 929.3 ± 70.55 ng/g (mean ± SEM, $n = 10$) and 1497 ± 110.2 ng/g (mean ± SEM, $n = 10$), respectively (see Figure 3). This suggests that **9Q** treatment enhances the cerebral acetylcholine level in 3xTg-AD mice.

2.3. Compound 9Q Ameliorated the Cognitive Deficits of 3xTg-AD Mice.

Twenty-four female 3xTg-AD mice were treated with designated dosing regimens for 4 weeks. We found that the body weight of the animals at week 4 changed slightly (with body weight changed by −8.4% for the control group, −4.1% for the **9Q** 3 mg/kg group, −4.3% for the **9Q** 10 mg/kg group, and −8.1% for the **9Q** 30 mg/kg group, compared with the initial weight), suggesting **9Q** was well tolerated. No significant alterations of the appearance and home-cage behavior were observed throughout the study.

MWM was used to evaluate the effects of **9Q** on the cognitive deficits of 3xTg-AD mice following 1 month treatment. The MWM task can reflect the memory and spatial learning of the mice. Compound **9Q** treatment (30 (mg/kg)/day, $n = 8$) significantly reduced the latency time (time to reach the platform) compared with the vehicle control on day 4 ($F(3, 28) = 3.9$, $P = 0.019$; see Figure 4A). Mice treated with **9Q** (30 (mg/kg)/day) spent significantly more time in the target quadrant ($F(3,28) = 3.263$, $P = 0.0429$; see Figure 4B) and performed significant more platform crossings ($F(3,28) = 4.046$, $P = 0.0204$; see Figure 4C) compared with the vehicle treated mice during the probe trial. These results suggested that **9Q** treatment ameliorated the cognitive impairments in the 3xTg-AD mice.

https://dx.doi.org/10.1021/acschemneuro.0c00464
ACS Chem. Neurosci. XXXX, XXX, XXX−XXX

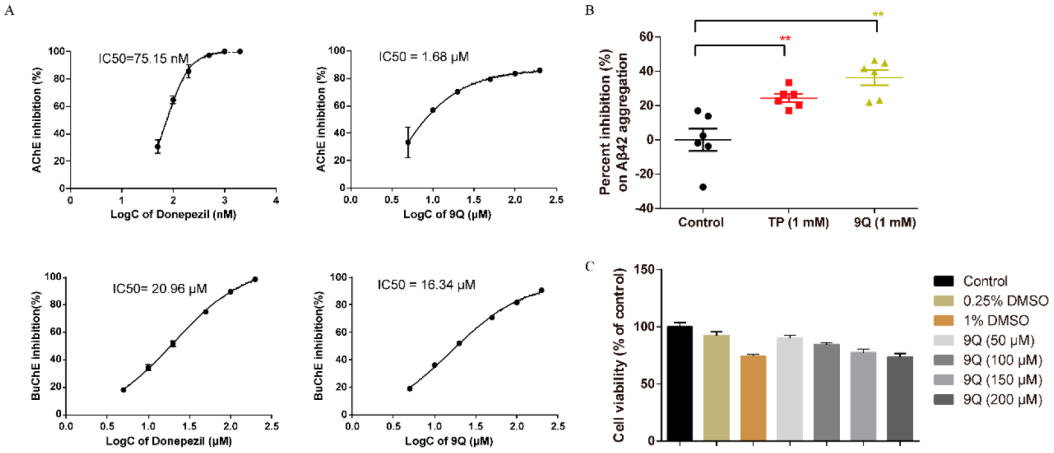

Figure 2. Compound **9Q** exhibited dual inhibition of ChE activity and Aβ42 aggregation and low cytotoxicity. (A) Compound **9Q** suppressed AChE and BuChE activities. The IC_{50} value of **9Q** on AChE or BuChE was determined using the Ellman's method. (B) Calculated inhibition percent of the compounds (1 mM) on Aβ42 aggregation at 12 h from initiation. TP represents tramiprosate. (C) Cell viability of SH-SY5Y cells in the presence of **9Q**. All data are presented as the mean ± SEM (n = 2 for panel A, n = 6 for panels B and C). Significance was analyzed by one-way ANOVA (for panel B) followed by Dunnett's multiple comparisons test using GraphPad Prism. *p < 0.01 compared with vehicle control group.

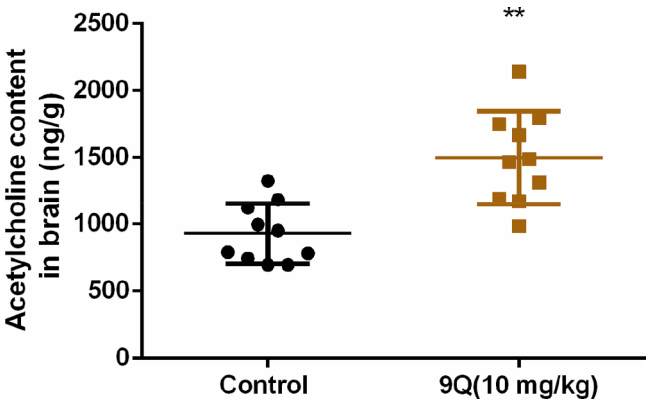

Figure 3. Compound **9Q** enhanced the cerebral acetylcholine level in 3xTg-AD mice. After 120 min treatment, the cerebral acetylcholine level was detected. All data are presented as the mean ± SEM (n = 10). Significance was analyzed by unpaired t test with Welch's correction using GraphPad Prism. *p < 0.01 compared with vehicle control group.

2.4. Compound 9Q Reduced the Cerebral Amyloid Burden. The Aβ42 level in brain homogenate guanidine hydrochloride fraction, which reflected the deposition of amyloid in brain, was detected by ELISA. As shown in Figure 5A, 1 month treatment with **9Q** (30 (mg/kg)/day) significantly decreased Aβ42 deposition in the brains of the 3xTg-AD mice compared with that of the vehicle control (F(3,20) = 5.953, P = 0.0045). Cerebral senile plaques were detected by IHC. Reduced cerebral plaques in hippocampus were also observed after one-month treatment with **9Q** via IHC staining (see Figure 5B). These results indicated that **9Q** treatment reduced the cerebral amyloid deposition in the 3xTg-AD mice.

2.5. Compound 9Q Mitigated Synaptic Dysfunction in the Brains of 3xTg-AD Mice. To assess the ability of **9Q** to reduce synapse loss in 3xTg-AD mice, the levels of postsynaptic and presynaptic proteins were investigated by using Western blotting and immunofluorescence (IF) staining. As shown in Figure 6A,B, **9Q** treatment elevated the expression of postsynaptic density 95 (PSD-95) and synaptophysin (SYP, an integral membrane glycoprotein that is localized in presynaptic vesicles of nerve cells) proteins compared with the vehicle group (F(3,12) = 22.86, P < 0.0001 for PSD-95; F(3,12) = 35.50, P < 0.0001 for SYP). SYP and PSD-95 in subiculum regions of the hippocampus were studied by IF staining (see Figure 6C,D). It is noted that the fluorescent signal of SYP or PSD-95 (red) in vicinity of the fluorescent signal of nuclei (blue) indicated SYP or PSD-95 positive. The images of SYP and PSD-95 were semiquantified by ImageJ software. From the relative integrated density (Figure 6E), though not statistically significant, enhancements of SYP and PSD-95 in **9Q** treated mice were observed. These results suggested that **9Q** exerted neuroprotective effects through enhancing the expression of synaptic proteins.

2.6. Compound 9Q Decreased APP Level by Regulating APP Processing in 3xTg-AD Mouse Brains. We then further explored the amyloid precursor protein (APP) and the processing protease level in mouse brains after one-month treatment with **9Q** by Western blotting. As shown in Figure 7, **9Q** treatment for one-month down-regulated APP level in 3xTg-AD mouse brains compared with vehicle control group (F(3,12) = 145.4, P = 0.0002). Meanwhile, ADAM17 (the regulated α-secretase of APP) and BACE (β-site amyloid precursor protein cleaving enzyme) were found to be up-regulated and down-regulated, respectively, in **9Q** treated mouse brains (F(3,12) = 45.71, P = 0.0015 for ADAM17; F(3,12) = 13.89, P = 0.0003 for BACE). The PSEN1 and PSEN2 protein levels were increased in **9Q** treated mice compared with the vehicle treated mice (F(3,12) = 275.3, P < 0.0001 for PSEN1; F(3,12) = 6.692, P = 0.0066 for BACE). These observations suggested that **9Q** decreased APP level by promoting the nonamyloidogenic pathway and inhibiting the amyloidogenic pathway.

2.7. Compound 9Q Alleviated Tau Pathology and Cdk5 Activity in 3xTg-AD Mice. Tau hyperphosphorylation is one of the important pathological hallmarks of AD. We detected phosphorylated tau in 3xTg-AD mice by IHC staining. Treatment with **9Q** reduced the phospho-tau (Ser202, Thr205) in mouse brains compared with the vehicle control (see Figure 8A). We also detected the tauopathy related protein levels in the brains of 3xTg-AD mice that were treated with **9Q** or PBS vehicle. As shown in Figure 8B,C, we

https://dx.doi.org/10.1021/acschemneuro.0c00464
ACS Chem. Neurosci. XXXX, XXX, XXX−XXX

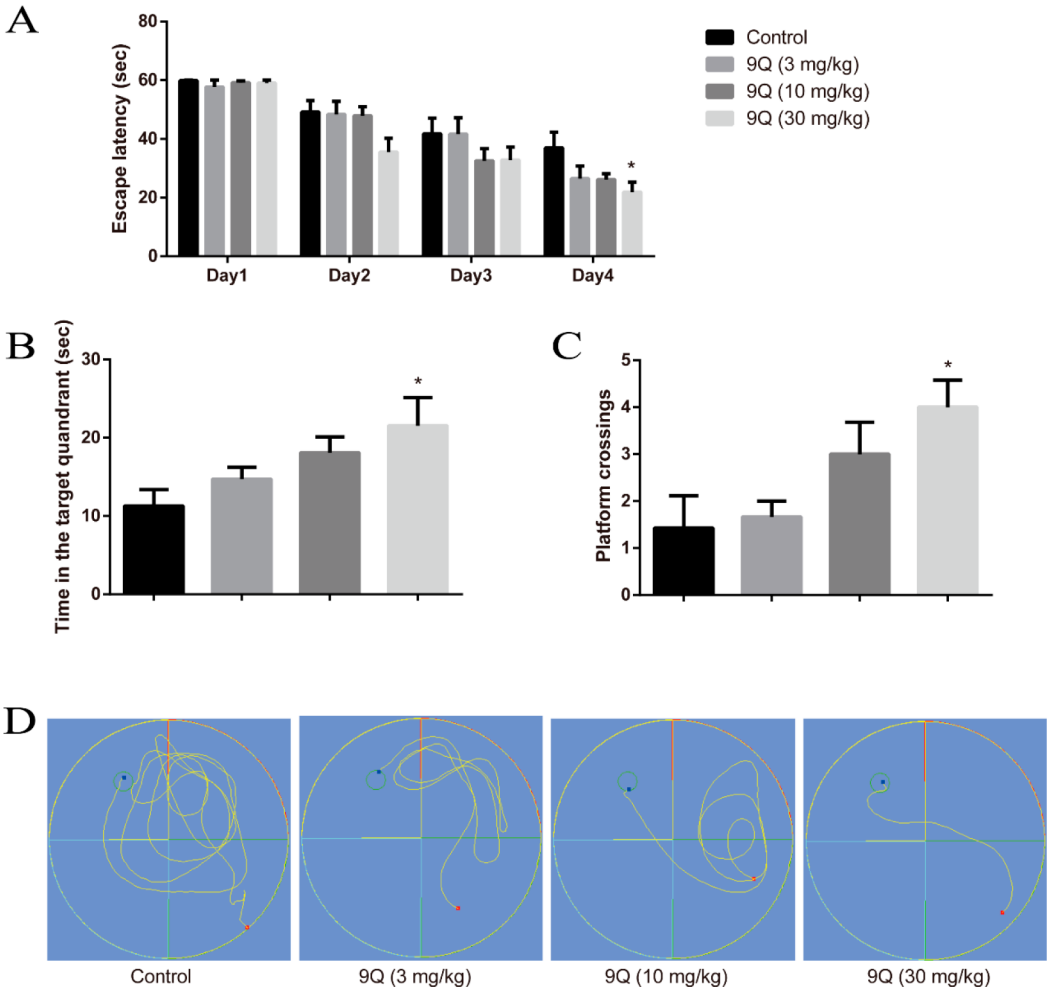

Figure 4. Compound **9Q** ameliorated the cognitive deficits in the MWM studies after one month treatment. (A) Latency to reach the escape platform. (B) Time spent in the platform quadrant within 1 min test on Day 5. (C) Number of platform crossings within 1 min test on Day 5. (D) Representative trajectories of the mice in the second acquisition study on day 4. All data are presented as the mean ± SEM (n = 8). Significance was analyzed by repeated-measures one-way ANOVA (for panel A) and one-way ANOVA (for panels B and C) followed by Dunnett's multiple comparisons test using GraphPad Prism. *p < 0.05 compared with vehicle treated Tg mice.

observed that **9Q** treatment significantly reduced the tau protein phosphorylation ($F(3,12) = 78.23$, $P < 0.0001$ for p-tau (Ser202, Thr205); $F(3,12) = 246.6$, $P < 0.0001$ for p-tau (Ser422); $F(3,12) = 32.56$, $P < 0.0001$ for p-tau (Thr212); $F(3,12) = 78.41$, $P < 0.0001$ for p-tau (Ser262)). Moreover, **9Q** was found to reduce the cyclin-dependent kinase 5 (Cdk5) protein level ($F(3, 12) = 19.38$, $P = 0.0005$; see Figures 8B,C).

2.8. Compound 9Q Attenuated OA-Induced Tau Hyperphosphorylation and Reduced Cdk5 Action in SH-SY5Y Cells. To corroborate the inhibitory effects of **9Q** on tau hyperphosphorylation and Cdk5 protein expression level *in vitro*, we performed our investigations using SH-SY5Y cell line. SH-SY5Y cells were incubated with okadaic acid (OA) to induce tau hyperphosphorylation. As shown in Figure 9A, 40 nM OA treatment induced phosphorylated tau in SH-SY5Y cell, while **9Q** treatment reversed tau phosphorylation. We also observed significantly decreased in Cdk5 and p35/25 protein expression levels in the **9Q** treatment group (see Figure 9A). Collectively, our results suggested that **9Q** inhibited tau hyperphosphorylation through the down regulation of Cdk5 activity in SH-SY5Y cells. To evaluate the neuroprotective effects of **9Q**, the OA treated SH-SY5Y cells were incubated with **9Q** (1, 2, or 5 μM) for 24 h. The cell viability was then evaluated by MTT assay. As shown in Figure 9B, **9Q** treatment significantly enhanced the cell viability of the OA-treated SH-SY5Y cells in a concentration-dependent manner ($F(3,20) = 21.14$, $p < 0.0001$).

3. DISCUSSION

The multifactorial etiology of AD has led to research into MTDLs as an emerging strategy to tackle this disease.[27,28] ChE inhibition is regarded as the most common approach that is available for AD treatment for now. The amyloid hypothesis is one of the most prevailing theories for AD etiology and has attracted considerable attention in AD drug discovery.[29,30] Recently, we have reported some dual inhibitors of ChE activity and Aβ aggregation.[25] We found that **9Q** outperformed donepezil in the inhibition of BuChE. It has been reported that BuChE was widely expressed in AD brains and contributed to the hydrolysis of acetylcholine.[8,31] Moreover, **9Q** outperformed tramiprosate,[26] an Aβ aggregation inhibitor that has entered phase III clinical trials, in suppressing Aβ aggregation. It should be pointed out that the *in vitro* assay to evaluate amyloid aggregation inhibition served to rank the potency of the compounds with respect to tramiprosate. Our assay appears to be sensitive at 1 mM compound

https://dx.doi.org/10.1021/acschemneuro.0c00464
ACS Chem. Neurosci. XXXX, XXX, XXX−XXX

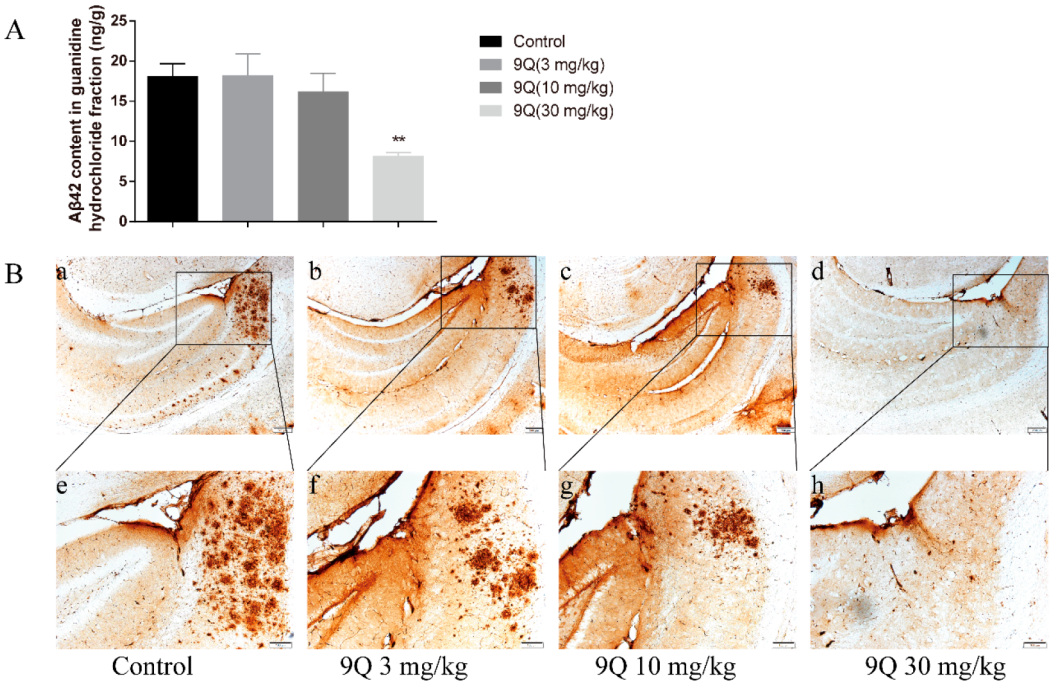

Figure 5. Compound **9Q** reduced brain amyloid burden (Aβ42 levels) following one month of treatment. (A) Levels of Aβ42 in the guanidine hydrochloride soluble fraction of brain tissue were detected by ELISA. All data are presented as the mean ± SEM (n = 6). Significance was analyzed by one-way ANOVA followed by Dunnett's multiple comparisons test using GraphPad Prism. **p < 0.01, compared with vehicle treated 3xTg-AD mice. (B) Representative images of hippocampus amyloid plaques detected by IHC. Scale bar 200 μm (for panels a−d) and 100 μm (for panels e−h).

concentration, taking into consideration of the inhibitory potency of tramiprosate. It is noted that at a concentration of 1 mM, **9Q** exerted obvious toxicity in the SH-SY5Y cell line, with cell viability only 27.5% (data not shown). However, **9Q** did not appear to be toxic in the SH-SY5Y cell line up to 200 μM in our cytotoxicity evaluation. Here we directed our attention to the *in vivo* pharmacological evaluation of **9Q**.

The 3xTg-AD mouse model used in the present study was generated by co-microinjection with APP and tau transgenes into single-cell embryos from homozygous PS1 (M146V) knockin mice.[32] The 3xTg-AD mouse develops progressively plaques and tangles and age-related synaptic dysfunction and cognitive deficits, which is a valuable model for AD therapeutic evaluation.[33,34] Prior to extensive *in vivo* studies, **9Q** was evaluated for BBB penetration. We found that **9Q** exhibited detectable brain exposure in 3xTg-AD mice. Following a single dose of **9Q** (10 mg/kg) to 3xTg-AD mice, concentrations of **9Q** were found to be 10.2 nM in plasma and 15.6 nM in brain at 2 h. Based on literature[35] and our previous report,[33] the Aβ concentrations in cerebrospinal fluid (CSF) of human and plasma in mouse were no more than 2 ng/mL and 20 ng/mL, which are equivalent to less than 0.4 nM and 4 nM, respectively. As shown in Figure 3, single-dose of **9Q** enhanced the cerebral acetylcholine level at 2 h, suggesting that **9Q** could reach the brain to modulate the cerebral metabolism of acetylcholine.

Next, we tested the pharmacodynamics effects of **9Q** in the 3xTg-AD mouse model. The Morris water maze (MWM) was designed to investigate the spatial learning and memory of rodents and was widely used in the neurocognitive treatment studies.[36] Using the MWM, we found that **9Q** treatment ameliorated the cognitive deficits in 3xTg-AD mice (see Figure 4). We then examined the Aβ42 deposition in mouse brains by ELISA and IHC. As shown in Figure 5, **9Q** reduced the amyloid burden in 3xTg-AD mice. From the above *in vitro* and *in vivo* studies, **9Q** was found to be a promising dual inhibitor of ChE activity and Aβ aggregation in 3xTg-AD mouse model.

As AD is a multifactorial disease, modification of a specific pathology may not necessarily lead to symptomatic improvements. We observed that one-month treatment with **9Q** ameliorated the cognitive deficits in 3xTg-AD mice which might be due to multifaceted roles of **9Q** in AD pathologies. AD is characterized as cognitive impairment and memory loss. Synapses are considered as the neurological basis of memory and learning.[37,38] Various synaptic marker proteins, such as PSD-95[39,40] and SYP,[41] were reported to be related to memory loss and cognitive deficits and were reduced in AD brains. Among the neuropathological features of the disease, synapse dysfunction correlated best with dementia.[42] As shown in Figure 6, **9Q** mitigated synapse loss in the brains of 3xTg-AD mice. Emerging evidence suggested that Aβ and tau accumulation contributed to synapse loss and the spread of pathology.[42,43] The lack of APP was found to be beneficial in the formation of synapse.[44] In the present study, the reduced APP level (Figure 7) and relieved tau pathology (Figure 8) were also observed in **9Q** treated 3xTg-AD mice.

In AD brains, APP is processed predominately by β-secretase and γ-secretase via the amyloidogenic pathway. As shown in Figure 7, the upregulation of ADAM17 (the regulated α-secretase) and down regulation of BACE indicated that **9Q** treatment regulated APP processing by promoting the nonamyloidogenic pathway and suppressing the amyloidogenic pathway. It is noted that, PSEN1 (presenilin 1) and PSEN2 (presenilin 2), the core proteins of γ-secretase, were upregulated in **9Q** treated 3xTg-AD mice. Point mutations in the PSEN genes increase APP cleavage resulting in excessive

https://dx.doi.org/10.1021/acschemneuro.0c00464
ACS Chem. Neurosci. XXXX, XXX, XXX−XXX

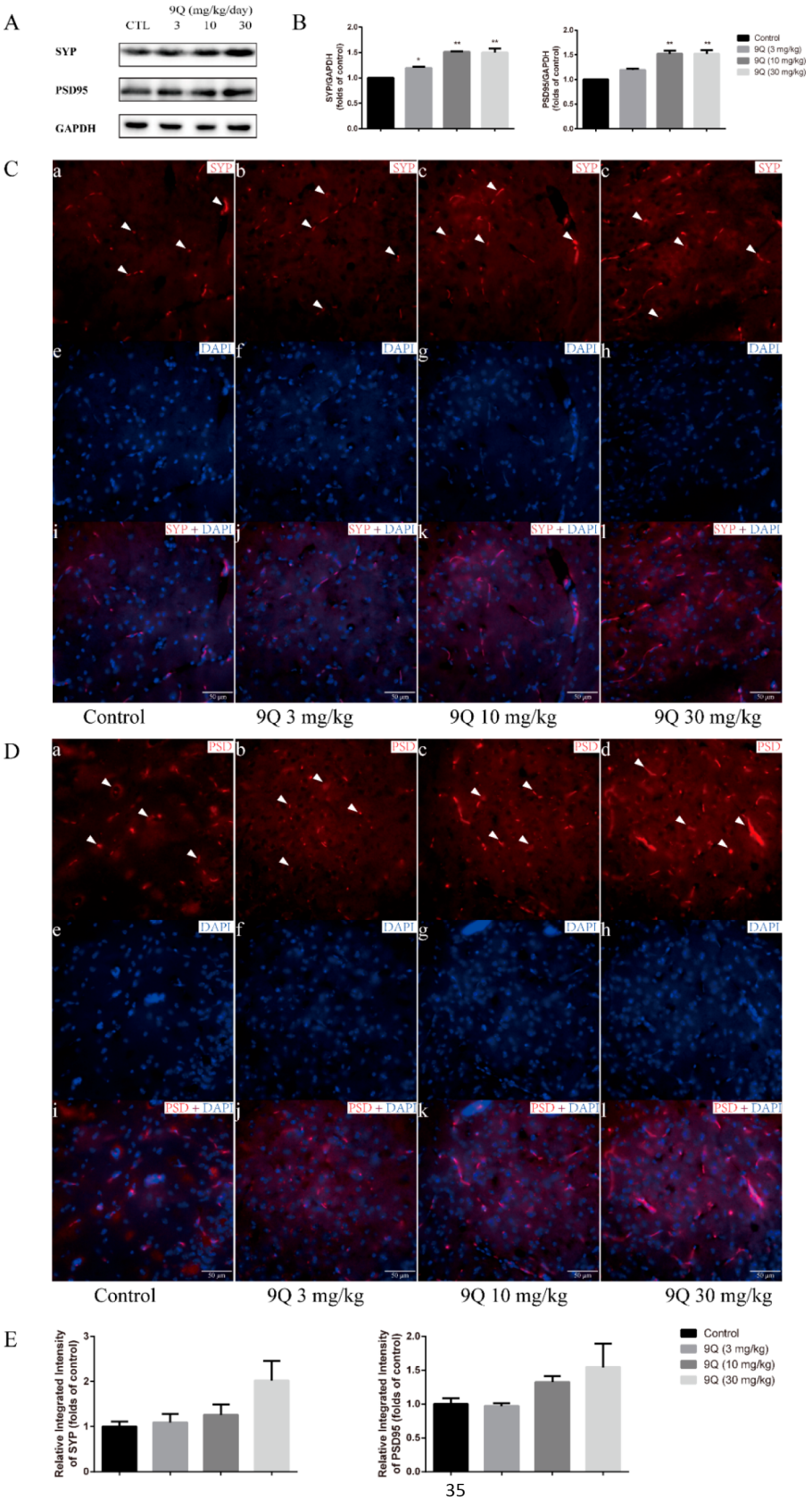

Figure 6. Compound **9Q** mitigated synaptic dysfunction in 3xTg-AD mouse brains following one month of treatment. (A) Representative Western blot of SYP, PSD-95, and GAPDH from brains of treated mice (PBS vehicle control and **9Q** treated at dosages of 3, 10, and 30 (mg/kg)/day). (B) Corresponding densitometry value ratios as mean ± SEM (n = 4). Significance was analyzed by one-way ANOVA followed by Dunnett's multiple comparisons test using GraphPad Prism. *p < 0.05, **p < 0.01, compared with vehicle treated 3xTg-AD mice. (C) Representative images of SYP in subiculum region of hippocampus studied by IF. (D) Representative images of PSD-95 in subiculum region of hippocampus studied by IF. Scale

https://dx.doi.org/10.1021/acschemneuro.0c00464
ACS Chem. Neurosci. XXXX, XXX, XXX−XXX

Figure 6. continued

bar 50 μm (for panels C and D). (E) Relative integrated density of the immunofluoroescent signals of panels C and D expressed as mean ± SEM (n = 4). Significance was analyzed by one-way ANOVA followed by Dunnett's multiple comparisons test using GraphPad Prism. No significant difference ($p \geq 0.05$) was observed compared with vehicle treated 3xTg-AD mice.

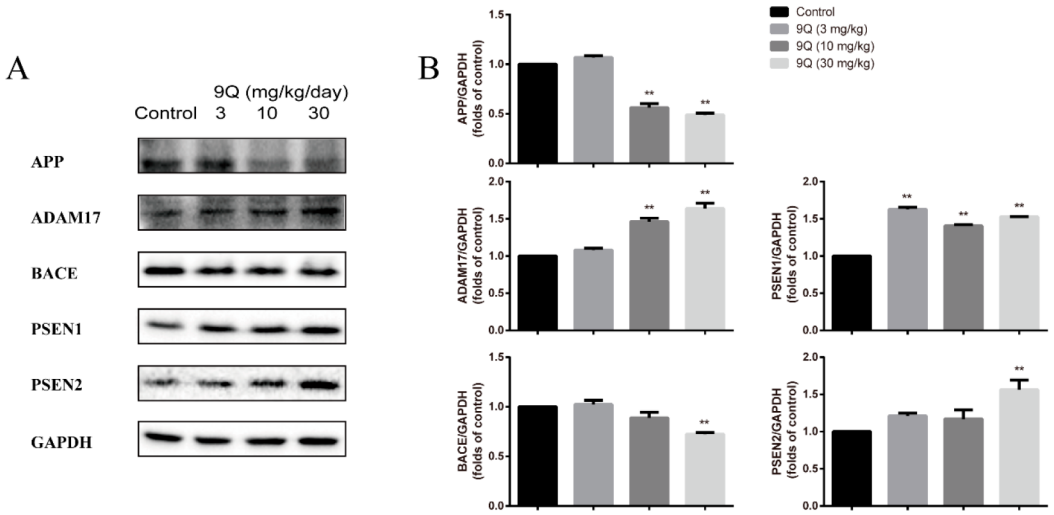

Figure 7. Compound **9Q** decreased APP level by regulating APP processing in 3xTg-AD mouse brains following one month of treatment. (A) Representative Western blot of APP, ADAM17, BACE, PSEN1, PSEN2, and GAPDH from brains of treated mice (PBS vehicle control and **9Q** treated at dosages of 3, 10, or 30 (mg/kg)/day). (B) The corresponding densitometry value ratios were the mean ± SEM (n = 4). Significance was analyzed by one-way ANOVA followed by Dunnett's multiple comparisons test using GraphPad Prism. $^{**}p < 0.01$, compared with vehicle treated 3xTg-AD mice.

Aβ, which would lead to familial AD cases.[45] According to our experimental data, though increasing γ-secretase was expressed in the brain (Figure 7), the amyloid burden was reduced instead (Figure 5).

Cdk5 is one of the cyclin-dependent kinases (Cdks), which has been reported to be closely related to the pathogenesis of AD.[46] Upon pathologic stimulus, Cdk5 became hyperactive, which led to aberrant hyperphosphorylation of tau and neurofilaments, resulting in neurodegeneration. Cdk5, as a tau kinase whose activity can be induced by Aβ peptides, connects the amyloid toxicity to tau hyperphosphorylation.[47] Aβ toxicity elevates the intraneuronal calcium concentration, which activates calpains to enhance the cleavage of p35 to p25.[46] The p25 binding to Cdk5 induces aberrant activity of Cdk5, which plays an important role in tauopathy in human and mouse models.[48] It is believed that Cdk5 may contribute to protein misfolding, toxicity, and undesirable interactions.[49] Targeting Cdk5/p25 might be a useful approach for treating AD.[50] Our results suggested that **9Q** reduced the Cdk5 activity on tau phosphorylation in 3xTg-AD mice (Figure 8). The effects of **9Q** on Cdk5 and tau phosphorylation was studied in SH-SY5Y cell line. Western blotting has shown that **9Q** significantly attenuated the tau hyperphosphorylation induced by OA (Figure 9A). Furthermore, the induction of Cdk5, p25, and p35 proteins confirmed the inhibitory effects of **9Q** on Cdk5 activity. It has been shown that **9Q** could protect SH-SY5Y cells against the toxicity induced by OA (Figure 9B). Clearly our studies manifested that the dual inhibition of ChE activity and Aβ aggregation could modulate the phenotypes of AD via multifaceted processes.

In conclusion, it has been shown that **9Q**, a dual inhibitor of ChEs and Aβ aggregation, enhanced the cerebral acetylcholine level and reduced the amyloid burden in 3xTg-AD mice. MWM studies revealed that **9Q** treatment for 1 month ameliorated the cognitive deficits in 3xTg-AD mice. It is noted that several pathological hallmarks of AD, namely, synapse dysfunction, amyloidogenic processing of APP and hyperphosphorylation of tau protein, were mitigated after 1 month treatment with **9Q** in 3xTg-AD mice. Taken together, our results suggested that **9Q** demonstrated efficacy in 3xTg-AD mouse model, which may provide new insights into the development of multifunctional agent to treat Alzheimer's disease.

4. EXPERIMENTAL PROCEDURES

4.1. Chemicals and Cell Culture. Compound **9Q** (Figure 1) was synthesized as previously described.[25] Donepezil and tramiprosate were purchased from Aladdin Co. (Shanghai, China). The human neuroblastoma SH-SY5Y cell line was a gift from Prof. Duncan Leung (Institute of Chinese Medical Sciences, University of Macau). The SH-SY5Y cells were cultured in humidified incubator at 37 °C with 5% CO_2. The cell culture medium was Dulbecco's modified Eagle's medium (DMEM, Gibco) containing 12% fetal bovine serum (FBS, Gibco) and 1% penicillin−streptomycin.

4.2. *In Vitro* AChE and BuChE Inhibition Assays. The inhibition of AChE and BuChE was measured by the Ellman method with modifications.[51] All reagents were prepared in a 0.1 M phosphate buffer at pH 8.0 with 1.6 mM $MgCl_2$ and 100 mM NaCl. In 200 μL AChE catalytic reaction system, 0.1 U/mL AChE (Sigma-Aldrich), 1 mM acetylthiocholine (ATC, Sigma-Aldrich), and 1.2 mM 5,5′-dithiobis(2-nitrobenzoic) acid (DTNB, Sigma-Aldrich) were incubated with **9Q** at different concentrations. In 200 μL BuChE catalytic reaction system, 0.05 U/mL BuChE (Sigma-Aldrich), 5 mM butyrylthiocholine (BTC, Sigma-Aldrich), and 6 mM DTNB were incubated with **9Q** at different concentrations. The reactions in 96-well plates were started by spiking the prewarmed ATC and BTC. Spectral data was recorded at 412 nm at 37 °C for 120 min by a plate reader (SpectraMax M5, Molecular Devices). All the experiments

https://dx.doi.org/10.1021/acschemneuro.0c00464
ACS Chem. Neurosci. XXXX, XXX, XXX−XXX

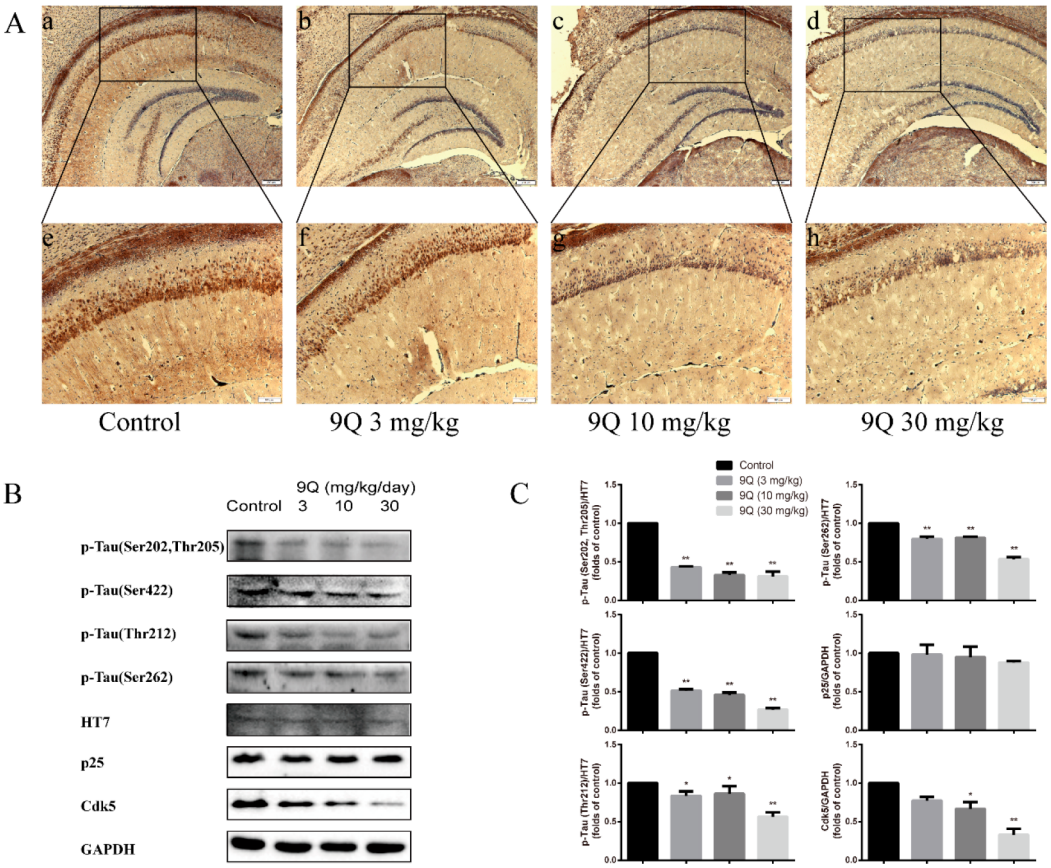

Figure 8. Compound **9Q** attenuated tau pathology and Cdk5 activity in 3xTg-AD mouse brains following one month of treatment. (A) Representative images of hippocampus phospho-tau detected by IHC. Scale bar 200 μm (for panels a−d) and 100 μm (for panels e−h). (B) Representative Western blot of p-Tau(Ser202, Thr205), p-Tau(Ser422), p-Tau(Thr212), p-Tau(Ser262), HT7, p25, Cdk5, and GAPDH from brains of treated mice (PBS vehicle control and **9Q** treated at dosages of 3, 10, or 30 mg/kg). (C) Corresponding densitometry value ratios as mean ± SEM (n = 4). Significance was analyzed by one-way ANOVA followed by Dunnett's multiple comparisons test using GraphPad Prism. *p < 0.05, **p < 0.01, compared with vehicle treated 3xTg-AD mice.

were carried out duplicate. Reactions without inhibitors were used to afford 100% AChE or BuChE activities. IC_{50} values were derived from the concentration−inhibition curve of the inhibitors by the GraphPad Prism program.

4.3. *In Vitro* Aβ Aggregation Inhibition Assay. The self-induced Aβ42 aggregation samples were prepared as previously described with modifications.[52] In brief, artificial Aβ42 peptides were solubilized in structure-breaking organic solvent 1,1,1,3,3,3-hexafluoro-2-propanol (HFIP, Sigma-Aldrich) at a concentration of 1 mg/mL to form the uniform Aβ42 monomer solution and then lyophilized.[53] The lyophilized Aβ42 peptides were solubilized in 0.05% ammonium hydroxide at 200 μM as the stock solution. The aggregation process in 20 μM Aβ42 peptide solution (in 20 mM sodium phosphate, pH 7.4) was initiated by adding solution containing 1 μM Aβ42 fibril seeds and 0.1 M NaCl. Compound **9Q** was then added, and the resulting solution was incubated without shaking at 37 °C.

The preparation of Aβ42 fibril seeding solution was accomplished by incubating 50 μM Aβ42 in 20 mM sodium phosphate buffer, pH 7.4, and 0.1 M NaCl in an incubator at 37 °C with continuous shaking at 80 rpm for 2 days. Then this 50 μM Aβ42 solution was sonicated for 30 min to generate the Aβ fibril seeds and stored at −20 °C for further usage.

The MALDI TOF MS (Microflex, Bruker) was used to determine the residual monomeric Aβ content in aggregating solutions. The detailed analytical method has been reported, and readers are directed to the literature for methodological details.[25]

4.4. Cell Viability Evaluation by MTT Assay. To test the cytotoxicity of the compounds, the viability of SH-SY5Y cells incubated with **9Q** was evaluated by the MTT assay. A concentration of 20 mM **9Q** was solubilized in DMSO as the stock solution. The SH-SY5Y cells were inoculated into 96-well plates at 40 000 cells per well containing 100 μL of medium. After 24 h, the culture medium was refreshed with addition of compound **9Q** at concentrations varying from 0 to 200 μM, and the cells were incubated for another 24 h. Then, each well was refreshed with medium containing 0.5 mg/mL MTT, and the cells were further incubated for 4 h at 37 °C. MTT solution was discarded, and 100 μL of DMSO was added into each well to enable complete solubilization of the formazan. The absorbance was measured at 590 nm with a plate reader (BioTek). Wells without cells were used as blanks and deducted as background from each sample. Inhibition was expressed as percentage of control. IC_{50} values were then derived from the concentration−inhibition curves by GraphPad Prism program.

To test the neuroprotective effects of **9Q** against tau hyperphosphorylation, the OA-induced SH-SY5Y cell hyperphosphorylation model was used.[54] After the SH-SY5Y cells were inoculated into 96-well plates and incubated for 24 h, the culture medium was refreshed with addition of both OA (40 nM) and **9Q** (0, 1, 2, 5 μM at one concentration) or none. After incubation for another 24 h, the medium was replaced with MTT solution. The experiment and the analysis were then performed as described before.

4.5. Cell Culture and Cell Protein Preparation for Western Blot. The SH-SY5Y cells were cultured in 10 cm Petri dish at 4 000 000 cells per dish in 10 mL of medium. After 24 h, the culture medium was refreshed with the addition of both OA (40 nM) and **9Q** (0, 1, 2, or 5 μM at one concentration) or none. After incubation for another 18 h, cells were harvested into 0.5 mL of ice-cold RIPA buffer

https://dx.doi.org/10.1021/acschemneuro.0c00464
ACS Chem. Neurosci. XXXX, XXX, XXX−XXX

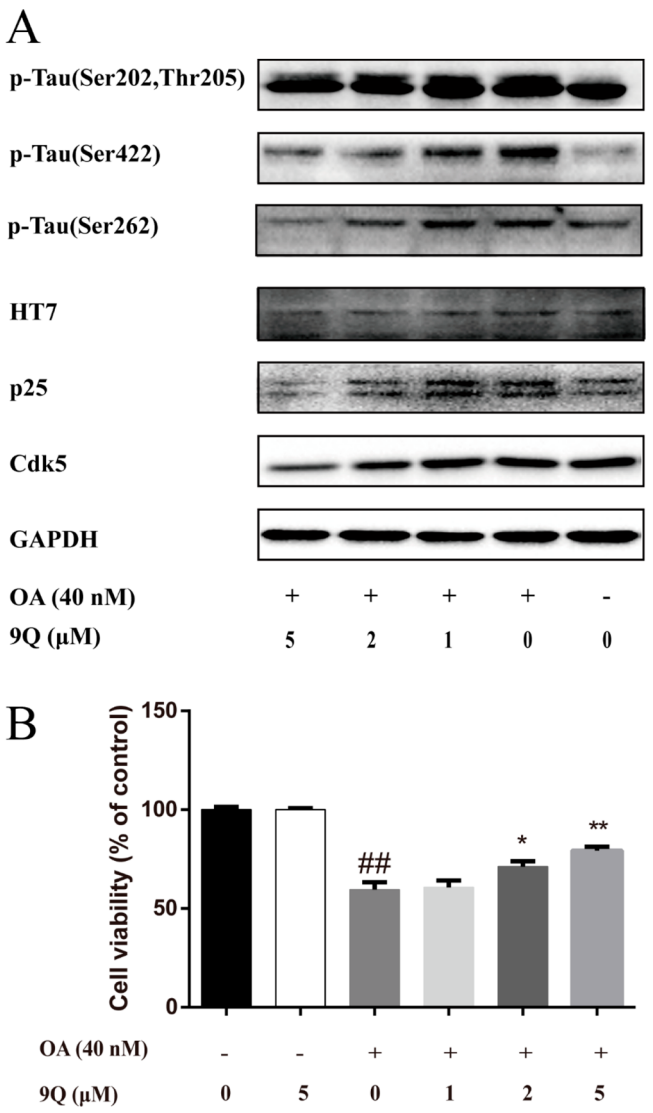

Figure 9. Compound **9Q** attenuated OA-induced tau hyperphosphorylation and reduced Cdk5 activity in SH-SY5Y cells. (A) Representative Western blot of p-Tau(Ser202, Thr205), p-Tau(Ser422), p-Tau(Ser262), HT7, p25, Cdk5, and GAPDH from SH-SY5Y cells treated with OA and **9Q**. (B) Viability of SH-SY5Y cells in the presence of OA and **9Q**. Significance was analyzed by one-way ANOVA followed by Dunnett's multiple comparisons test using GraphPad Prism. *$p < 0.05$, **$p < 0.01$, compared with OA alone treatment group, ##$p < 0.01$, compared with no-treatment group.

(50 mM Tris-HCl, 150 mM NaCl, 0.5% sodium deoxycholate, 1% Triton X-100, 0.1% SDS, pH 7.5) containing protease inhibitor cocktail (S8830, Sigma) and phosphatase inhibitor cocktail (04906845001, Roche) and mixed by gently rotation for 30 min at 4 °C. The supernatant was collected for Western blot assay by centrifuging the sample at 12 000*g* for 20 min at 4 °C.

4.6. Animals. The homozygous 3xTg-AD mice (B6; 129-Psen1tm1MpmTg (APPSwe, tauP301L) 1Lfa/Mmjax) were obtained from the Jackson Laboratory (Bar Harbor, Maine, USA) and maintained by the Animal Facility in the Faculty of Health Sciences (University of Macau). Twenty 10-month old 3xTg-AD mice (10 male and 10 female) were used in the study of **9Q** brain exposure and *in vivo* ChE inhibitory effect. Twenty-four 10-month old female 3xTg-AD mice were used in the **9Q** treatment study. The animal study protocols (#UMARE-AMEND-086 and #UMARE-AMEND-087) were approved by the Animal Research Ethics Committee of the University of Macau.

4.7. Brain Exposure of Compound 9Q in 3xTg-AD Mice. *4.7.1. Animal Dosing and Sample Collection.* Twenty 10-month old male and female mice were fasted but allowed free access to water for 24 h before dosing. Compound **9Q** was solubilized in PBS at 1 mg/mL and intraperitoneally (ip) injected to mice ($n = 10$) at a dose of 10 mg/kg. PBS as the vehicle control was injected to mice at a dose of 10 mL/kg. Blood (20 μL) was sampled via caudal vein to heparinized microcentrifuge tubes at a time point 120 min from dosing. The animals were then immediately terminated by CO_2 asphyxiation, and their brains were collected and stored at −80 °C for further analysis. Plasma was separated by centrifuging the blood sample at 1500*g*, 4 °C, for 20 min and stored in −80 °C for further analyses.

*4.7.2. Detection of **9Q** in Plasma and Brain Samples by LC-MS/MS.* Plasma and brain samples were prepared using the protocols previously described[55] and analyzed by LC-MS/MS (Waters, TQD) as previously described.[56] Readers are directed to the relevant literature for methodological details.

Compound **9Q** (m/z 299 > 130 as quantifier ion and m/z 299 > 142 as qualifier ion) and berberine (as internal standard, m/z 336 > 320 as quantifier ion and m/z 336 > 278 as qualifier ion) were simultaneously monitored via positive ionization mode.

4.8. Detection of Cerebral Acetylcholine. The brain samples in section 4.7.1 were used to evaluate the cerebral acetylcholine content. All LC-MS/MS conditions were the same as that for **9Q** detection, except that acetylcholine was monitored using m/z 146 > 87 as quantifier ion and m/z 146 > 60 as qualifier ion.

4.9. Compound 9Q Treatment in 3xTg-AD Mice. Twenty-four female 3xTg-AD mice (10 months old) were separated randomly into 4 groups. Group 1 was the PBS vehicle control group and groups 2−4 were, respectively, low (3 mg/kg), middle (10 mg/kg), and high (30 mg/kg) **9Q**-dosing groups. Compound **9Q** was freshly prepared in PBS buffer every day for dosing. These mice were dosed intraperitoneally once a day for 5 days per week (five consecutive dosing days followed by two rest days) for one month. Food and water consumption was monitored periodically. Body weights were recorded weekly.

4.10. Morris Water Maze (MWM). After the 3xTg-AD mice were treated with **9Q** for one month, MWM tests were performed with the ZS Dichuang (Beijing, China) MWM equipment containing a Xeye Aba video tracking system to assess memory and learning as described previously.[33] Briefly, mice were trained to locate the invisible submerged platform (8 cm in diameter) in the MWM circular pool (120 cm in diameter and 60 cm in height). The 2860 Bt7200 video tracking camera was mounted directly above the center of the pool to monitor activity within the pool. The temperature (22 °C) and decorations of the pool as well as the location of the platform were maintained constant throughout the mice training period.

During the acquisition phase, mice were trained for 4 consecutive days with 4 trials per day at 4 starting points (E, SE, NW, and N) to find the submerged platform in opaque water. When a mouse located the platform in 60 s, the mouse could stay on the platform for 5 s before being returned to its home cage. Otherwise, the mouse would be gently guided to the platform and allowed to stay on it for 15 s. The time required to find the platform (escape latency) was recorded. On day 5, the probe trial without the submerged platform was performed. In the 60 s probe trial, the mouse was freely allowed to explore in the pool. Time spent in the target quadrant where the submerged platform was located and the time that the mouse passed across the platform (platform crossings) were recorded by the tracking system.

4.11. Brain Sample Preparation. After the MWM studies, the mice were terminated by CO_2 asphyxiation, and immediately their brains were collected. The left-brain hemispheres were fixed in 4% paraformaldehyde (PFA) for 48 h and dehydrated in 30% sucrose for 72 h for immunostaining. The right-brain hemispheres were frozen in liquid nitrogen and stored at −80 °C for later protein extraction. Brain proteins were extracted as previously described with some modification.[33] Briefly, the right-brain hemisphere was homogenized and fractionated into three parts (1) TBS-soluble fraction, (2) RIPA soluble fraction, and (3) guanidine hydrochloride soluble fraction.

https://dx.doi.org/10.1021/acschemneuro.0c00464
ACS Chem. Neurosci. XXXX, XXX, XXX−XXX

The brain hemisphere was homogenized in 4 vol (w/v) of ice-cold TBS containing protease inhibitor cocktail (S8830, Sigma) and phosphatase inhibitor cocktail (04906845001, Roche) with a high-throughput tissuelyser (Scientz-192) at 15 times/second for 1 min in a 4 °C room. Samples were centrifuged (16 000*g*, 30 min at 4 °C), and the TBS-soluble fraction was collected and stored at −80 °C. The pellet was then rehomogenized in 4 vol of ice-cold RIPA buffer containing protease inhibitor cocktail and phosphatase inhibitor cocktail at 25 times/second for 2 min and mixed gently by rotation at 4 °C for 30 min. Samples were centrifuged (16 000*g*, 30 min at 4 °C), and the RIPA soluble fraction was collected for Western blot assay. The pellet was then resuspended in 5 M guanidine hydrochloride/50 mM Tris-HCl, pH 7.5, to 150 mg/mL (based on pellet weight) and mixed by rotation for 2 h at room temperature. Samples were centrifuged (16 000*g*, 30 min at 4 °C), and the guanidine hydrochloride fraction was collected and frozen.

4.12. Enzyme-Linked Immunosorbent Assay (ELISA). The guanidine hydrochloride soluble fraction of the brain tissue was used for detection of Aβ42 deposition in brain. The mouse specific Aβ42 ELISA kit was obtained from Invitrogen (KMB3441). The experiment was operated as the product manual described. Plates were analyzed using a plate reader (SpectraMax M5, Molecular Devices).

4.13. Western Blot Assay. The brain homogenate RIPA soluble fraction and cell lysates were separately used to study the expression levels of various proteins. Protein concentrations were assessed by Pierces BCA Protein Assay Kit (Thermo Fisher Scientific). All samples were mixed with 5× sample buffer (250 mM Tris-HCl, pH 6.8, 8% SDS, 50% glycerol, 500 mM dithiothreitol (DTT), and 0.02% bromophenol blue) and boiled for 5 min at 100 °C. Samples containing an equal amount of protein were separated by SDS-PAGE and transferred onto poly(vinylidene difluoride) (PVDF) membrane. The membrane was blocked in 5% bovine serum albumin (BSA) for 2 h and incubated with desired primary antibodies overnight, followed by anti-rabbit or anti-mouse HRP-conjugated secondary antibody (Cell Signaling Technology) for 2 h. Membranes were finally visualized in a ChemiDoc MP Imaging System (Bio-Rad) after 2 min incubation in ECL Substrate (6883S, Cell Signaling Technology). The primary antibodies used for detection were as follows: anti-APP antibody (2452s, Cell Signaling Technology), anti-ADAM antibody (ab39162, Abcam), anti-BACE antibody (5606p, Cell Signaling Technology), anti-presenilin 1 antibody (5643P, Cell Signaling Technology), anti-presenilin 2 antibody (9979p, Cell Signaling Technology), anti-PSD 95 antibody (3450s, Cell Signaling Technology), anti-synaptophysin (AB9272, Millipore), anti-phospho-tau (Ser202/Thr205) antibody (MN1020, ThermoFisher), anti-phospho-tau (Ser422) antibody (44-764G, ThermoFisher), anti-phospho-tau (Thr212) antibody (44-740G, ThermoFisher), anti-phospho-tau (Ser262) antibody (OPA103142, ThermoFisher), anti-tau antibody (MN1000, ThermoFisher), anti-p35/25 antibody (2680s, Cell Signaling Technology), anti-Cdk5 antibody (2506s, Cell Signaling Technology), anti-GAPDH antibody (5174s, Cell Signaling Technology). Western blot images were analyzed by ImageJ software (National Institutes of Health, USA) to quantify the band signal intensity.

4.14. Immunostaining. Coronal sections of the left hemisphere of mouse brains were collected using a cryotome cryostat (CM5030, Leica). The 20 μM thick coronal sections were inserted onto slides for Aβ42 and phosphorylated tau detection by IHC, while SYP and PSD-95 detections were accomplished by IF. The slides were air-dried at room temperature overnight and then stored at −80 °C until further usage. At the beginning of the immunostaining, slides were all fixed in cold acetone at −20 °C for 15 min.

4.14.1. Immunohistochemistry (IHC). The IHC study was performed for Aβ42 and phospho-tau detection. In Aβ42 detection, antigen retrieval was carried out by soaking the sections with 90% formic acid for 8 min. In phosphorylated tau detection, antigen retrieval was carried out by heating the sections in sodium citrate buffer (10 mM sodium citrate, 0.05% Tween 20, pH 6.0) using the 2100 antigen retriever (Aptum), followed with permeabilization by incubating the sections in PBS with 0.5% Triton X-100 for 20 min. Sections were then blocked in PBS with 3% BSA at room temperature for 1 h and incubated with the primary anti-Aβ42 antibody (805502, Biolegend) or primary anti-phospho-tau (Ser202/Thr205) antibody (MN1020, ThermoFisher) in PBS with 3% BSA at 4 °C overnight. Sections were then incubated with 3% hydrogen peroxide followed by biotinylated secondary antibody (31800, ThermoFisher) for 30 min at room temperature. In the above operations, sections were washed 2 times in PBS with 0.2% Triton X-100 for 5 min before commencing the next incubation procedure. ABC kit (32020, ThermoFisher) and DAB quanto (TA-060-QHDX, ThermoFisher) were applied to visualize brain sections. Hematoxylin was used to counterstain for phospho-tau detection. Images of the IHC sections were acquired using an Olympus BX53 system microscope equipped with Olympus DP73 digital camera.

4.14.2. Immunofluorescence (IF). The IF was performed for SYP and PSD-95 detection. After antigen retrieval, permeabilization, blocking, and incubation with primary anti-SYP antibody (AB9272, Millipore) or primary anti-PSD-95 antibody (3450s, Cell Signaling Technology) in the same procedure as for phospho-tau detection introduced in section 4.14.1, sections were incubated with the Alexa Fluor 594 cross-adsorbed secondary antibody (A11012, ThermoFisher) for 30 min at room temperature. In the above operations, sections were washed 2 times in PBS with 0.2% Triton X-100 for 5 min before commencing the next incubation procedure. DAPI was used to counterstain. Images of the sections were acquired using a Nikon Ti-E fluorescent microscope equipped with Nikon DS-Qi2 digital camera. Signals of SYP and PSD-95 positive in IF images were quantified by ImageJ software.

4.15. Statistical Analysis. Statistical analyses were carried out using GraphPad Prism (version 6.02, San Diego, CA, USA). The **9Q** content data was expressed as mean ± standard deviation (SD), and other data was expressed as mean ± standard error of the mean (SEM). Unpaired *t* test with Welch's correction was used for cerebral acetylcholine level data analysis, repeated-measures one-way variance (ANOVA) followed by Dunnett's multiple comparisons test was used to analyze the data obtained from MWM study, and one-way ANOVA followed by Dunnett's multiple comparisons test was used for other data analysis. Data with $p \leq 0.05$ was considered significant.

AUTHOR INFORMATION

Corresponding Author

Kin Yip Tam − *Faculty of Health Sciences, University of Macau, Taipa, Macau, China;* orcid.org/0000-0001-5507-8524; Email: kintam@um.edu.mo

Authors

Yaojun Ju − *Faculty of Health Sciences, University of Macau, Taipa, Macau, China*

Harapriya Chakravarty − *Faculty of Health Sciences, University of Macau, Taipa, Macau, China*

Complete contact information is available at: https://pubs.acs.org/10.1021/acschemneuro.0c00464

Author Contributions

Y.J. performed experiments, including animal work, biochemistry, IHC, and IF, and analyzed the data. Y.J. and K.Y.T. discussed the results and composed and edited the manuscript. H.C. performed chemical synthesis. K.Y.T. supervised all phases of the study.

Notes

The authors declare no competing financial interest.

ACKNOWLEDGMENTS

We thank Dr. Xiaohui Hu for helpful suggestions and discussion throughout this project. We thank Prof. Duncan Leung (ICMS, University of Macau) for a sample of SH-SY5Y

cells. We thank the Animal Research Core and Biological Imaging & Stem Cell Core at Faculty of Heath Sciences, University of Macau, for technical support. This work was funded by University of Macau (File no. MYRG2016-00102-FHS).

■ ABBREVIATIONS

AD, Alzheimer's disease; Aβ, amyloid beta; AChE, acetylcholinesterase; BuChE, butyrylcholinesterase; APP, amyloid precursor protein; BBB, blood−brain barrier; NMDAR, *N*-methyl-D-aspartate receptor; MTDL, multitarget-directed ligand; ATC, acetylthiocholine; DTNB, 5,5′-dithiobis(2-nitrobenzoic) acid; BTC, butyrylthiocholine; HFIP, 1,1,1,3,3,3-hexafluoro-2-propanol; MALDI, matrix-assisted laser desorption ionization; CHCA, α-cyano-4-hydroxycinnamic acid; TFA, trifluoroacetic acid; OA, okadaic acid; MWM, Morris water maze; PFA, paraformaldehyde; DTT, dithiothreitol; PVDF, poly(vinylidene difluoride); BSA, bovine serum albumin; IHC, immunohistochemistry; SYP, synaptophysin; PSD-95, postsynaptic density 95; IF, immunofluorescence; APP, amyloid precursor protein; BACE, β-site amyloid precursor protein cleaving enzyme; Cdk5, cyclin-dependent kinase 5

■ REFERENCES

(1) Cummings, J., Aisen, P. S., DuBois, B., Frölich, L., Jack, C. R., Jones, R. W., Morris, J. C., Raskin, J., Dowsett, S. A., and Scheltens, P. (2016) Drug development in Alzheimer's disease: the path to 2025. *Alzheimer's Res. Ther. 8* (1), 39.

(2) Zemek, F., Drtinova, L., Nepovimova, E., Sepsova, V., Korabecny, J., Klimes, J., and Kuca, K. (2014) Outcomes of Alzheimer's disease therapy with acetylcholinesterase inhibitors and memantine. *Expert Opin. Drug Saf. 13* (6), 759−74.

(3) Kumar, A., Singh, A., and Ekavali (2015) A review on Alzheimer's disease pathophysiology and its management: an update. *Pharmacol. Rep. 67* (2), 195−203.

(4) Savelieff, M. G., Nam, G., Kang, J., Lee, H. J., Lee, M., and Lim, M. H. (2019) Development of Multifunctional Molecules as Potential Therapeutic Candidates for Alzheimer's Disease, Parkinson's Disease, and Amyotrophic Lateral Sclerosis in the Last Decade. *Chem. Rev. 119* (2), 1221−1322.

(5) Wilcock, G. K., Esiri, M. M., Bowen, D. M., and Smith, C. C. (1982) Alzheimer's disease. Correlation of cortical choline acetyltransferase activity with the severity of dementia and histological abnormalities. *J. Neurol. Sci. 57* (2−3), 407−17.

(6) Wilkinson, D. G., Francis, P. T., Schwam, E., and Payne-Parrish, J. (2004) Cholinesterase inhibitors used in the treatment of Alzheimer's disease: the relationship between pharmacological effects and clinical efficacy. *Drugs Aging 21* (7), 453−78.

(7) Mesulam, M. M., Guillozet, A., Shaw, P., Levey, A., Duysen, E. G., and Lockridge, O. (2002) Acetylcholinesterase knockouts establish central cholinergic pathways and can use butyrylcholinesterase to hydrolyze acetylcholine. *Neuroscience 110* (4), 627−39.

(8) Mesulam, M., Guillozet, A., Shaw, P., and Quinn, B. (2002) Widely spread butyrylcholinesterase can hydrolyze acetylcholine in the normal and Alzheimer brain. *Neurobiol. Dis. 9* (1), 88−93.

(9) DeBay, D. R., Reid, G. A., Macdonald, I. R., Mawko, G., Burrell, S., Martin, E., Bowen, C. V., and Darvesh, S. (2017) Butyrylcholinesterase-knockout reduces fibrillar beta-amyloid and conserves (18)FDG retention in 5XFAD mouse model of Alzheimer's disease. *Brain Res. 1671*, 102−110.

(10) Darvesh, S. (2016) Butyrylcholinesterase as a Diagnostic and Therapeutic Target for Alzheimer's Disease. *Curr. Alzheimer Res. 13* (10), 1173−7.

(11) Gabriel, A. J., Almeida, M. R., Ribeiro, M. H., Duraes, J., Tabuas-Pereira, M., Pinheiro, A. C., Pascoal, R., Santana, I., and Baldeiras, I. (2017) Association between butyrylcholinesterase and cerebrospinal fluid biomarkers in Alzheimer's disease patients. *Neurosci. Lett. 641*, 101−106.

(12) Selkoe, D. J., and Hardy, J. (2016) The amyloid hypothesis of Alzheimer's disease at 25 years. *EMBO Mol. Med. 8* (6), 595−608.

(13) Soldano, A., and Hassan, B. A. (2014) Beyond pathology: APP, brain development and Alzheimer's disease. *Curr. Opin. Neurobiol. 27*, 61−7.

(14) Laird, F. M., Cai, H., Savonenko, A. V., Farah, M. H., He, K., Melnikova, T., Wen, H., Chiang, H. C., Xu, G., Koliatsos, V. E., Borchelt, D. R., Price, D. L., Lee, H. K., and Wong, P. C. (2005) BACE1, a major determinant of selective vulnerability of the brain to amyloid-beta amyloidogenesis, is essential for cognitive, emotional, and synaptic functions. *J. Neurosci. 25* (50), 11693−709.

(15) Hardy, J., and Allsop, D. (1991) Amyloid deposition as the central event in the aetiology of Alzheimer's disease. *Trends Pharmacol. Sci. 12* (10), 383−8.

(16) Choi, M. L., and Gandhi, S. (2018) Crucial role of protein oligomerization in the pathogenesis of Alzheimer's and Parkinson's diseases. *FEBS J. 285* (19), 3631−3644.

(17) Salahuddin, P., Fatima, M. T., Abdelhameed, A. S., Nusrat, S., and Khan, R. H. (2016) Structure of amyloid oligomers and their mechanisms of toxicities: Targeting amyloid oligomers using novel therapeutic approaches. *Eur. J. Med. Chem. 114*, 41−58.

(18) Giorgetti, S., Greco, C., Tortora, P., and Aprile, F. A. (2018) Targeting Amyloid Aggregation: An Overview of Strategies and Mechanisms. *Int. J. Mol. Sci. 19* (9), 2677.

(19) Mohamed, T., Shakeri, A., and Rao, P. P. (2016) Amyloid cascade in Alzheimer's disease: Recent advances in medicinal chemistry. *Eur. J. Med. Chem. 113*, 258−72.

(20) Wang, T., Liu, X. H., Guan, J., Ge, S., Wu, M. B., Lin, J. P., and Yang, L. R. (2019) Advancement of multi-target drug discoveries and promising applications in the field of Alzheimer's disease. *Eur. J. Med. Chem. 169*, 200−223.

(21) Jankowska, A., Wesolowska, A., Pawlowski, M., and Chlon-Rzepa, G. (2018) Multi-Target-Directed Ligands Affecting Serotonergic Neurotransmission for Alzheimer's Disease Therapy: Advances in Chemical and Biological Research. *Curr. Med. Chem. 25* (17), 2045−2067.

(22) Mezeiova, E., Spilovska, K., Nepovimova, E., Gorecki, L., Soukup, O., Dolezal, R., Malinak, D., Janockova, J., Jun, D., Kuca, K., and Korabecny, J. (2018) Profiling donepezil template into multipotent hybrids with antioxidant properties. *J. Enzyme Inhib. Med. Chem. 33* (1), 583−606.

(23) Unzeta, M., Esteban, G., Bolea, I., Fogel, W. A., Ramsay, R. R., Youdim, M. B., Tipton, K. F., and Marco-Contelles, J. (2016) Multi-Target Directed Donepezil-Like Ligands for Alzheimer's Disease. *Front. Neurosci. 10*, 205.

(24) Wang, Y., Wang, H., and Chen, H. Z. (2016) AChE Inhibition-based Multi-target-directed Ligands, a Novel Pharmacological Approach for the Symptomatic and Disease-modifying Therapy of Alzheimer's Disease. *Curr. Neuropharmacol. 14* (4), 364−75.

(25) Chakravarty, H., Ju, Y., Chen, W.-H., and Tam, K. Y. (2020) Dual targeting of cholinesterase and amyloid beta with pyridinium/isoquinolium derivatives. *Drug Dev. Res. 81* (2), 242−255.

(26) Hey, J. A., Yu, J. Y., Versavel, M., Abushakra, S., Kocis, P., Power, A., Kaplan, P. L., Amedio, J., and Tolar, M. (2018) Clinical Pharmacokinetics and Safety of ALZ-801, a Novel Prodrug of Tramiprosate in Development for the Treatment of Alzheimer's Disease. *Clin. Pharmacokinet. 57* (3), 315−333.

(27) Gong, C. X., Liu, F., and Iqbal, K. (2018) Multifactorial Hypothesis and Multi-Targets for Alzheimer's Disease. *J. Alzheimer's Dis. 64* (s1), S107−s117.

(28) Rosini, M., Simoni, E., Minarini, A., and Melchiorre, C. (2014) Multi-target design strategies in the context of Alzheimer's disease: acetylcholinesterase inhibition and NMDA receptor antagonism as the driving forces. *Neurochem. Res. 39* (10), 1914−23.

(29) Rafii, M. S., and Aisen, P. S. (2015) Advances in Alzheimer's disease drug development. *BMC Med. 13*, 62.

https://dx.doi.org/10.1021/acschemneuro.0c00464
ACS Chem. Neurosci. XXXX, XXX, XXX−XXX

(30) Mangialasche, F., Solomon, A., Winblad, B., Mecocci, P., and Kivipelto, M. (2010) Alzheimer's disease: clinical trials and drug development. *Lancet Neurol. 9* (7), 702−16.
(31) Geula, C., and Darvesh, S. (2004) Butyrylcholinesterase, cholinergic neurotransmission and the pathology of Alzheimer's disease. *Drugs Today 40* (8), 711−21.
(32) Oddo, S., Caccamo, A., Shepherd, J. D., Murphy, M. P., Golde, T. E., Kayed, R., Metherate, R., Mattson, M. P., Akbari, Y., and LaFerla, F. M. (2003) Triple-transgenic model of Alzheimer's disease with plaques and tangles: intracellular Abeta and synaptic dysfunction. *Neuron 39* (3), 409−21.
(33) Wu, X., Kosaraju, J., Zhou, W., and Tam, K. Y. (2018) SLOH, a carbazole-based fluorophore, mitigates neuropathology and behavioral impairment in the triple-transgenic mouse model of Alzheimer's disease. *Neuropharmacology 131*, 351−363.
(34) Sah, S. K., Lee, C., Jang, J. H., and Park, G. H. (2017) Effect of high-fat diet on cognitive impairment in triple-transgenic mice model of Alzheimer's disease. *Biochem. Biophys. Res. Commun. 493* (1), 731−736.
(35) Bibl, M., Mollenhauer, B., Esselmann, H., Lewczuk, P., Klafki, H. W., Sparbier, K., Smirnov, A., Cepek, L., Trenkwalder, C., Rüther, E., Kornhuber, J., Otto, M., and Wiltfang, J. (2006) CSF amyloid-beta-peptides in Alzheimer's disease, dementia with Lewy bodies and Parkinson's disease dementia. *Brain 129*, 1177−87.
(36) D'Hooge, R., and De Deyn, P. P. (2001) Applications of the Morris water maze in the study of learning and memory. *Brain Res. Rev. 36* (1), 60−90.
(37) Mayford, M., Siegelbaum, S. A., and Kandel, E. R. (2012) Synapses and memory storage. *Cold Spring Harbor Perspect. Biol. 4* (6), a005751.
(38) Langille, J. J., and Brown, R. E. (2018) The Synaptic Theory of Memory: A Historical Survey and Reconciliation of Recent Opposition. *Front. Syst. Neurosci. 12*, 52.
(39) Whitfield, D. R., Vallortigara, J., Alghamdi, A., Howlett, D., Hortobagyi, T., Johnson, M., Attems, J., Newhouse, S., Ballard, C., Thomas, A. J., O'Brien, J. T., Aarsland, D., and Francis, P. T. (2014) Assessment of ZnT3 and PSD95 protein levels in Lewy body dementias and Alzheimer's disease: association with cognitive impairment. *Neurobiol. Aging 35* (12), 2836−2844.
(40) Sultana, R., Banks, W. A., and Butterfield, D. A. (2009) Decreased Levels of PSD95 and Two Associated Proteins and Increased Levels of BCl2 and Caspase 3 in Hippocampus from Subjects with Amnestic Mild Cognitive Impairment: Insights into Their Potential Roles for Loss of Synapses and Memory, Accumulation of A beta, and Neurodegeneration in a Prodromal Stage of Alzheimer's Disease. *J. Neurosci. Res. 88* (3), 469−477.
(41) Yuki, D., Sugiura, Y., Zaima, N., Akatsu, H., Takei, S., Yao, I., Maesako, M., Kinoshita, A., Yamamoto, T., Kon, R., Sugiyama, K., and Setou, M. (2015) DHA-PC and PSD-95 decrease after loss of synaptophysin and before neuronal loss in patients with Alzheimer's disease. *Sci. Rep. 4*, 9.
(42) Li, K., Wei, Q., Liu, F. F., Hu, F., Xie, A. J., Zhu, L. Q., and Liu, D. (2018) Synaptic Dysfunction in Alzheimer's Disease: Abeta, Tau, and Epigenetic Alterations. *Mol. Neurobiol. 55* (4), 3021−3032.
(43) Spires-Jones, T. L., and Hyman, B. T. (2014) The intersection of amyloid beta and tau at synapses in Alzheimer's disease. *Neuron 82* (4), 756−71.
(44) Priller, C., Bauer, T., Mitteregger, G., Krebs, B., Kretzschmar, H. A., and Herms, J. (2006) Synapse formation and function is modulated by the amyloid precursor protein. *J. Neurosci. 26* (27), 7212−21.
(45) Newman, M., Musgrave, I. F., and Lardelli, M. (2007) Alzheimer disease: amyloidogenesis, the presenilins and animal models. *Biochim. Biophys. Acta, Mol. Basis Dis. 1772* (3), 285−97.
(46) Liu, S. L., Wang, C., Jiang, T., Tan, L., Xing, A., and Yu, J. T. (2016) The Role of Cdk5 in Alzheimer's Disease. *Mol. Neurobiol. 53* (7), 4328−42.
(47) Lee, M. S., and Tsai, L. H. (2003) Cdk5: one of the links between senile plaques and neurofibrillary tangles? *J. Alzheimer's Dis. 5* (2), 127−37.
(48) Seo, J., Kritskiy, O., Watson, L. A., Barker, S. J., Dey, D., Raja, W. K., Lin, Y. T., Ko, T., Cho, S., Penney, J., Silva, M. C., Sheridan, S. D., Lucente, D., Gusella, J. F., Dickerson, B. C., Haggarty, S. J., and Tsai, L. H. (2017) Inhibition of p25/Cdk5 Attenuates Tauopathy in Mouse and iPSC Models of Frontotemporal Dementia. *J. Neurosci. 37* (41), 9917−9924.
(49) Wilkaniec, A., Czapski, G. A., and Adamczyk, A. (2016) Cdk5 at crossroads of protein oligomerization in neurodegenerative diseases: facts and hypotheses. *J. Neurochem. 136* (2), 222−33.
(50) Bhounsule, A. S., Bhatt, L. K., Prabhavalkar, K. S., and Oza, M. (2017) Cyclin dependent kinase 5: A novel avenue for Alzheimer's disease. *Brain Res. Bull. 132*, 28−38.
(51) Ellman, G. L., Courtney, K. D., Andres, V., and Featherstone, R. M. (1961) A new and rapid colorimetric determination of acetylcholinesterase activity. *Biochem. Pharmacol. 7* (2), 88−95.
(52) Xue, C., Lin, T. Y., Chang, D., and Guo, Z. (2017) Thioflavin T as an amyloid dye: fibril quantification, optimal concentration and effect on aggregation. *R. Soc. Open Sci. 4* (1), 160696.
(53) Broersen, K., Jonckheere, W., Rozenski, J., Vandersteen, A., Pauwels, K., Pastore, A., Rousseau, F., and Schymkowitz, J. (2011) A standardized and biocompatible preparation of aggregate-free amyloid beta peptide for biophysical and biological studies of Alzheimer's disease. *Protein Eng., Des. Sel. 24* (9), 743−50.
(54) Kamat, P. K., Rai, S., Swarnkar, S., Shukla, R., and Nath, C. (2014) Molecular and cellular mechanism of okadaic acid (OKA)-induced neurotoxicity: a novel tool for Alzheimer's disease therapeutic application. *Mol. Neurobiol. 50* (3), 852−65.
(55) Zhou, W., Hu, X. H., and Tam, K. Y. (2017) Systemic clearance and brain distribution of carbazole-based cyanine compounds as Alzheimer's disease drug candidates. *Sci. Rep. 7*, 10.
(56) Zhou, W., Wu, X. L., Li, J., Hu, X. H., and Tam, K. Y. (2016) Quantification of permanent positively charged compounds in plasma using one-step dilution to reduce matrix effect in MS. *Bioanalysis 8* (6), 497−509.

https://dx.doi.org/10.1021/acschemneuro.0c00464
ACS Chem. Neurosci. XXXX, XXX, XXX−XXX